

Insight into the factors influencing NMR parameters in crystalline materials from the KF-YF₃ binary system

Jamal Dabachi, Monique Body, Jens Dittmer, Aydar Rakhmatullin, Franck Fayon, and Christophe Legein

Electronic Supplementary Information

Table of contents

Fig. S1. Euler angles (α , β , γ) describing the relative orientation of the chemical shift tensor in the EFG principal axis frame.	3
Fig. S2. Experimental and calculated XRPD diagrams of K ₂ YF ₅ .	3
Fig. S3. Perspective views of K ₂ YF ₅ structure showing the chains of YF ₇ monocapped octahedra and corrugated sheets of KF ₈ polyhedra.	4
Table S1. Atom, atomic coordinates and anisotropic or isotropic displacement parameters determined from the Rietveld refinement of the K ₂ YF ₅ XRPD pattern and bond valence sum (BVS). Atomic coordinates, BVS and displacements after PBE-DFT optimization of the atomic positions.	4
Table S2. Space group and cell parameters of structures used in DFT-PAW/GIAW calculations of NMR parameters.	5
Table S3. Experimental and PBE-DFT geometry-optimized fractional atomic coordinates, and corresponding atomic displacements for γ -K ₃ YF ₆ .	5
Table S4. Experimental and PBE-DFT geometry-optimized fractional atomic coordinates, and corresponding atomic displacements for KYF ₄ .	6
Table S5. Experimental and PBE-DFT geometry-optimized fractional atomic coordinates, and corresponding atomic displacements for β -KY ₂ F ₇ .	7
Table S6. Experimental and PBE-DFT geometry-optimized fractional atomic coordinates, and corresponding atomic displacements for α -KY ₃ F ₁₀ .	7
Table S7. Experimental and PBE-DFT geometry-optimized fractional atomic coordinates, and corresponding atomic displacements for YF ₃ .	7
Table S8. Compound, Y site and environment, minimum and average Y-F distances deduced from ES and APO structures.	8
Table S9. Compound, K site and environment, minimum and average K-F distances deduced from ES and APO structures.	8
Fig. S4. Experimental and fitted ¹⁹ F MAS NMR spectra of γ -K ₃ YF ₆ .	9
Table S10. ¹⁹ F isotropic chemical shift, chemical shift anisotropy, asymmetry parameters, line width and relative intensity determined from reconstruction of the ¹⁹ F NMR spectrum of γ -K ₃ YF ₆ .	9
Fig. S5. Experimental and fitted ¹⁹ F MAS NMR spectra of K ₂ YF ₅ .	10
Table S11. ¹⁹ F isotropic chemical shift, chemical shift anisotropy, asymmetry parameter, line width and relative intensity determined from reconstruction of the ¹⁹ F NMR spectrum of K ₂ YF ₅ .	10
Fig. S6. Experimental and fitted ¹⁹ F MAS NMR spectra of KYF ₄ .	11
Table S12. ¹⁹ F isotropic chemical shift, chemical shift anisotropy, asymmetry parameter, line width and relative intensity determined from reconstruction of the ¹⁹ F NMR spectrum of KYF ₄ .	11
Fig. S7. ¹⁹ F “infinite spinning rate” isotropic spectrum issued from the TOP processing of the conventional MAS spectrum and experimental and fitted MAS NMR spectra of β -KY ₂ F ₇ .	12

Table S13. ^{19}F isotropic chemical shift, chemical shift anisotropy, asymmetry parameter, line width and relative intensity determined from reconstruction of the ^{19}F NMR spectrum of $\beta\text{-KY}_2\text{F}_7$.	13
Fig. S8. Experimental and fitted ^{19}F MAS NMR spectra of KY_3F_{10} .	14
Table S14. ^{19}F isotropic chemical shift, chemical shift anisotropy, asymmetry parameter, line width and relative intensity determined from reconstruction of the ^{19}F NMR spectrum of $\alpha\text{-KY}_3\text{F}_{10}$.	14
Table S15. Phase, F site and multiplicity, ^{19}F σ_{iso} , σ_{csa} and η values issued from DFT-GIPAW calculations for APO structures of KF, $\gamma\text{-K}_3\text{YF}_6$, K_2YF_5 , $\alpha\text{-KY}_3\text{F}_{10}$ and YF_3 and calculated ^{19}F δ_{iso} (ppm) values for $\gamma\text{-K}_3\text{YF}_6$, K_2YF_5 and $\alpha\text{-KY}_3\text{F}_{10}$.	14
Table S16. F site, ^{19}F σ_{iso} and calculated δ_{iso} , σ_{csa} and η values issued from DFT-GIPAW calculations for APO structures of $\beta\text{-KY}_2\text{F}_7$.	15
Table S17. F site, cationic environment, and multiplicity, ^{19}F σ_{iso} , σ_{csa} and η values issued from DFT-GIPAW calculations for APO structures of KYF_4 .	15
Fig. S9. Experimental and fitted ^{89}Y MAS NMR spectrum of YF_3 , $\gamma\text{-K}_3\text{YF}_6$, K_2YF_5 , KYF_4 , $\beta\text{-KY}_2\text{F}_7$ and $\alpha\text{-KY}_3\text{F}_{10}$.	16
Table S18. Phase, NMR line, ^{89}Y δ_{iso} , line width and relative intensity determined from reconstruction of the ^{89}Y NMR spectra of KF-YF ₃ binary system.	17
Fig. S10. Experimental and fitted ^{39}K MAS NMR of KF and $\alpha\text{-KY}_3\text{F}_{10}$.	18
Table S19. Phase, K site, ^{39}K EFG tensor components and Euler angle values issued from DFT-GIPAW calculations for APO structures.	18
Table S20. Eigenvectors of the calculated ^{39}K EFG tensor, expressed in the crystallographic axis, for K1 in K_2YF_5 (APO), K1 and K2 in $\gamma\text{-K}_3\text{YF}_6$ (APO), and K2 in KYF_4 (APO).	18
Table S20. F-K1-F angles between two adjacent K-F bonds for K1F ₆ octahedron in APO structure of $\gamma\text{-K}_3\text{YF}_6$.	19
Fig. S11. Experimental and theoretical ^{39}K MAS NMR spectra of K_2YF_5 , $\gamma\text{-K}_3\text{YF}_6$, $\beta\text{-KY}_2\text{F}_7$ and $\gamma\text{-K}_3\text{YF}_6$.	19

1. Euler Angles

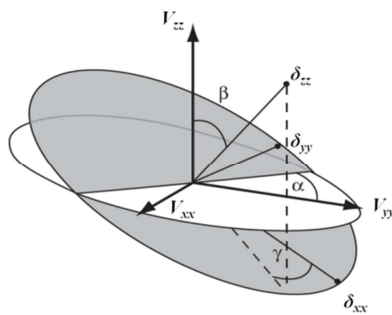


Fig. S1. Euler angles (α , β , γ) describing the relative orientation of the chemical shift tensor in the EFG principal axis frame.

2. Structural refinement of K_2YF_5 structure

The K_2YF_5 structure was initially refined in the orthorhombic $Pna2_1$ (33) space group,¹ however a structural refinement on powder XRD was later achieved in the orthorhombic $Pnma$ (62) space group.² This space group was then confirmed by an EPR study, from the Y site symmetry.³ However, this structure presents inconsistent average Y-F distances. A Rietveld refinement has been achieved using (i) the cell parameters of K_2YF_5 determined in the $Pna2_1$ space group¹ and interchanging a and b values and (ii) the atomic positions of K_2GdF_5 ⁴ interchanging the y and z atomic positions.⁴ The background level was modelled manually. Anisotropic displacement parameters (ADP) for yttrium and potassium, isotropic displacement parameters (IDP) for fluorine were also refined. The presence of KY_3F_{10} as impurity in the K_2YF_5 sample was taken into account for the final Rietveld refinements (Fig. S2). Satisfactory reliability factors were obtained: $R_{wp} = 0.12$, $R_{exp} = 0.041$, $R_{Bragg} = 0.055$. The refined cell parameters are: $a = 10.8002(3)$ Å, $b = 7.2707(2)$ Å and $c = 6.6010(2)$ Å. These values are similar to those of K_2YF_5 in $Pna2_1$ space group.¹ Atomic positions, ADP or IDP and bond valence sum^{5,6} are gathered in Table S1.

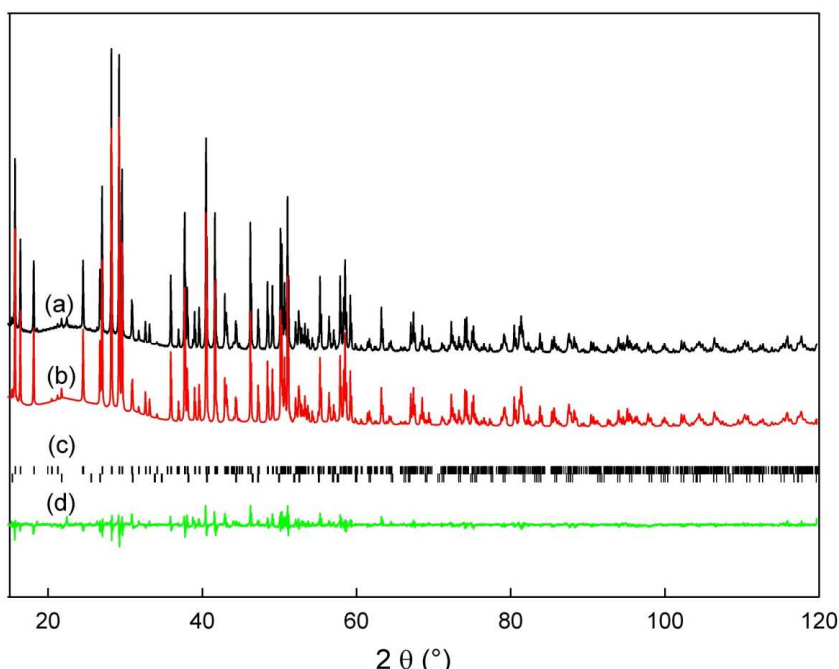


Fig. S2. Experimental (a) and calculated (b) XRPD diagrams of K_2YF_5 . The Bragg positions (c) of K_2YF_5 (above) and KY_3F_{10} (below) and the difference between experimental and calculated diagrams (d) are shown.

In this structure, the yttrium atoms are hepta-coordinated by fluorine atoms forming monocapped octahedra (Fig. S3a). These YF_7 polyhedra share opposite F2-F2 edges and form infinite chains along the b axis. Each potassium atom is coordinated to eight fluorine atoms. These KF_8 polyhedra are connected by theirs (F1, F3, F4) and (F2, F3, F4) faces along the b and c directions respectively, forming corrugated sheets in the (b, c) plane. These sheets are linked together in the a direction by shared F1-F1 edges (Fig. S3b) forming distorted hexagonal circles in the (a, b) plane.

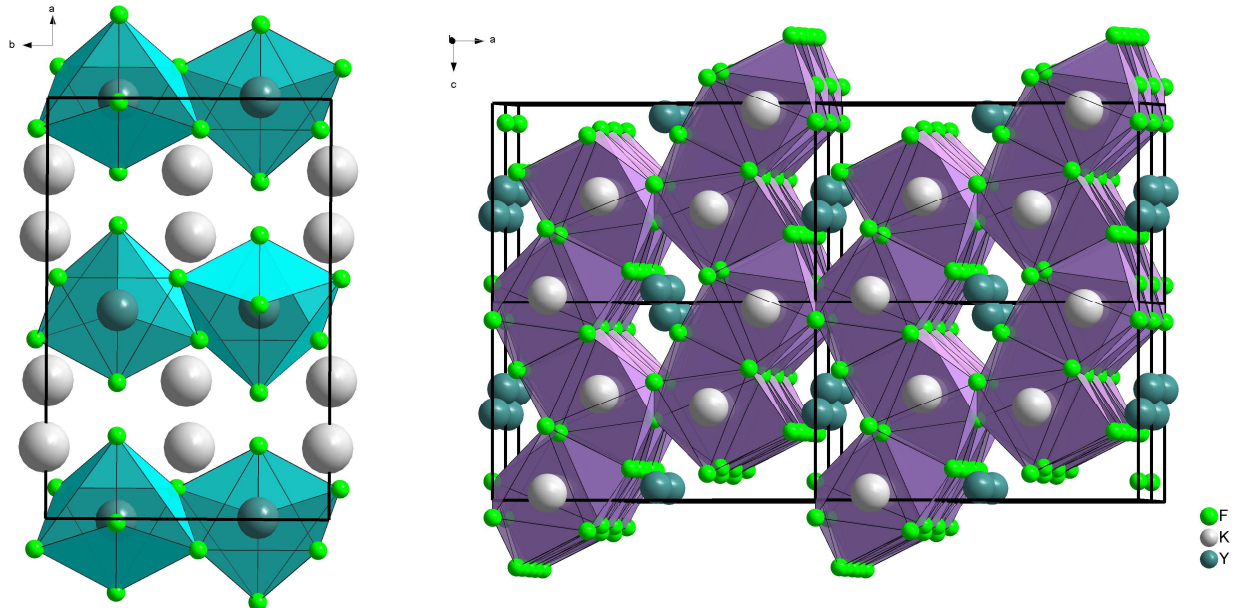


Fig. S3. Perspective views of K_2YF_5 structure showing the chains of YF_7 monocapped octahedra (left) and corrugated sheets of KF_8 polyhedra (right).

Table S1. Atom, atomic coordinates and anisotropic (U_{ii} , \AA^2) or isotropic (U_{iso} , \AA^2) displacement parameters determined from the Rietveld refinement of the K_2YF_5 powder XRD pattern and bond valence sum (BVS). Atomic coordinates, BVS and displacements (d , \AA) after PBE-DFT optimization of the atomic positions (italic).

Atom	Site	<i>x</i>	<i>y</i>	<i>z</i>	U_{11}	U_{22}	U_{33}	U_{iso}	BVS	<i>d</i>
Y1	4c	0.5036(7) 0.50316	1/4 1/4	0.0646(5) 0.06562	0.008(8)	0.003(1)	0.006(1)		2.61 2.90	0.008
K1	8d	0.6699(4) 0.67216	0.4938(14) 0.49208	0.5331(11) 0.53027	0.019(7)	0.011(8)	0.007(6)		1.06 1.03	0.033
F1	4c	0.5103 (32) 0.51258	1/4 1/4	0.4053(23) 0.39711				0.036(6)	0.90 1.05	0.059
F2	8d	0.4270(12) 0.42389	0.4617(19) 0.46426	0.8430(20) 0.85199				0.034(5)	0.92 0.96	0.071
F3	4c	0.6749(17) 0.66855	1/4 1/4	0.8696(27) 0.87329				0.024(2)	0.85 0.90	0.072
F4	4c	0.3035(18) 0.30720	1/4 1/4	0.1627(30) 0.16380				0.021(2)	0.99 1.03	0.041

3. DFT calculations

Table S2. Space group and cell parameters of structures used in DFT-PAW/GIPAW calculations of NMR parameters.

Compound	Space group	<i>a</i> (Å)	<i>b</i> (Å)	<i>c</i> (Å)	α (°)	β (°)	γ (°)	Ref.	ICSD
KF	<i>Fm-3m</i> (225)	5.367	5.367	5.367	90	90	90	[7]	52241
γ -K ₃ YF ₆	<i>P2₁/n</i> (14)	6.3376	6.5435	9.0390	90	90.65	90	[8]	416296
K ₂ YF ₅	<i>Pnma</i> (62)	10.800	7.271	6.601	90	90	90	this work	
KYF ₄	<i>P3₂</i> (145)	14.163	14.163	10.190	90	90	120	[9]	187000
β -KY ₂ F ₇	<i>Cm</i> (8)	14.291	7.979	11.984	90	125.14	90	[10]	n.a. *
α -KY ₃ F ₁₀	<i>Fm-3m</i> (225)	11.553	11.553	11.553	90	90	90	[11]	409643
YF ₃	<i>Pnma</i> (62)	6.3537	6.8545	4.3953	90	90	90	[12]	6023

*from NIMS Materials Database.

Table S3. Experimental (*x*, *y*, *z*)⁸ and PBE-DFT geometry-optimized (*x'*, *y'*, *z'*) fractional atomic coordinates, and corresponding atomic displacements (*d*, Å) for γ -K₃YF₆.

Atom	Site	<i>x</i>	<i>y</i>	<i>z</i>	<i>x'</i>	<i>y'</i>	<i>z'</i>	<i>d</i>
Y1	2a	0	0	0	0	0	0	0.000
K1	2b	1/2	1/2	0	1/2	1/2	0	0.000
K2	4e	0.01253	0.54757	-0.25335	0.01039	0.54995	-0.25692	0.038
F1	4e	0.2205	0.3255	0.5466	0.21750	0.32421	0.54760	0.023
F2	4e	0.3332	0.7726	0.5682	0.33185	0.77495	0.56926	0.020
F3	4e	0.3905	0.5574	0.2763	0.38896	0.55825	0.27443	0.020

Table S4. Experimental (x , y , z)⁹ and PBE-DFT geometry-optimized (x' , y' , z') fractional atomic coordinates, and corresponding atomic displacements (d , Å) for KYF_4 .

Atom	Site	x	y	z	x'	y'	z'	d
Y1	3a	0.13055	0.89040	0.66619	0.13057	0.88960	0.66631	0.011
Y2	3a	0.28078	0.73037	0.67411	0.28230	0.73136	0.67532	0.023
Y3	3a	0.78105	0.20748	0.65710	0.78015	0.20640	0.65639	0.016
Y4	3a	0.94103	0.05768	0.66979	0.94290	0.05948	0.67179	0.033
Y5	3a	0.45274	0.54494	0.67143	0.45230	0.54361	0.67167	0.017
Y6	3a	0.60289	0.38552	0.65198	0.60393	0.38608	0.65113	0.015
K1	3a	0.26672	0.21929	0.64643	0.26557	0.21639	0.64610	0.036
K2	3a	0.78083	0.71936	0.67589	0.78072	0.71902	0.67668	0.009
K3	3a	0.61130	0.87785	0.65016	0.61393	0.87659	0.64989	0.032
K4	3a	0.10466	0.39538	0.67984	0.10480	0.39505	0.67929	0.007
K5	3a	0.45608	0.06437	0.68040	0.45673	0.06190	0.68175	0.034
K6	3a	0.94765	0.56221	0.65014	0.94750	0.56181	0.65011	0.005
F1	3a	0.1309	0.9354	0.8839	0.13171	0.93463	0.88388	0.011
F2	3a	0.0702	0.8784	0.4569	0.06965	0.87876	0.45643	0.008
F3	3a	0.20735	0.59552	0.5238	0.20999	0.59487	0.52682	0.046
F4	3a	0.3388	0.72858	0.3409	0.33885	0.72959	0.34133	0.015
F5	3a	0.7377	0.2036	0.4403	0.73832	0.20484	0.43926	0.019
F6	3a	0.78924	0.2701	0.8667	0.78958	0.26944	0.86562	0.014
F7	3a	-0.0014	0.05974	0.3346	-0.00170	0.06057	0.33414	0.011
F8	3a	0.0761	-0.04768	0.1866	0.07730	-0.04489	0.18994	0.048
F9	3a	0.3917	0.5369	0.4623	0.39171	0.53754	0.46130	0.014
F10	3a	0.4571	0.5913	0.8881	0.45737	0.59018	0.88852	0.015
F11	3a	0.54783	0.29041	0.4623	0.54687	0.29080	0.46156	0.014
F12	3a	-0.2663	-0.60517	0.3190	-0.26359	-0.60531	0.32125	0.044
F13	3a	0.7667	0.72828	0.9313	0.76481	0.72804	0.93100	0.025
F14	3a	0.8094	0.72448	0.4231	0.80721	0.72328	0.42174	0.030
F15	3a	0.24799	0.22319	0.3903	0.24765	0.22230	0.38888	0.018
F16	3a	0.8089	0.0749	0.5653	0.80962	0.07467	0.56558	0.009
F17	3a	0.13261	0.39378	0.4279	0.13070	0.39406	0.42795	0.025
F18	3a	0.09371	0.40422	0.9355	0.09194	0.40421	0.93369	0.031
F19	3a	0.15200	0.75538	0.5730	0.15281	0.75494	0.57202	0.014
F20	3a	0.5900	0.88469	0.3935	0.59043	0.88409	0.39292	0.010
F21	3a	0.93653	0.5753	0.3960	0.93893	0.57789	0.39602	0.035
F22	3a	-0.4102	-0.94313	0.2380	-0.40828	-0.94248	0.23808	0.024
F23	3a	0.4854	0.06895	0.4277	0.48427	0.06930	0.42682	0.017
F24	3a	0.4524	0.08634	0.9383	0.45247	0.08646	0.93808	0.003

Table S5. Experimental (x , y , z)¹⁰ and PBE-DFT geometry-optimized (x' , y' , z') fractional atomic coordinates, and corresponding atomic displacements (d , Å) for $\beta\text{-KY}_2\text{F}_7$.

Atom	Site	x	y	z	x'	y'	z'	d
Y1	4b	0.1129	0.25956	0.3870	0.11967	0.25801	0.38897	0.086
Y2	4b	0.1137	0.2367	0.7052	0.11499	0.23670	0.70614	0.015
Y3	4b	0.1186	0.2377	0.0689	0.11868	0.23697	0.06873	0.006
Y4	2a	0.3575	0	0.7109	0.35845	0	0.71019	0.011
Y5	2a	0.8760	0	0.0684	0.87629	0	0.06596	0.027
K1	2a	0.3455	0	0.0423	0.35146	0	0.04628	0.070
K2	2a	0.3792	0	0.4001	0.38251	0	0.40175	0.039
K3	2a	0.8549	0	0.3582	0.85222	0	0.36055	0.032
K4	2a	0.8798	0	0.7377	0.88290	0	0.73455	0.038
F1	4b	0.003	0.239	0.161	0.00028	0.23814	0.15108	0.102
F2	4b	0.018	0.230	0.476	0.01565	0.23302	0.47072	0.057
F3	4b	0.115	0.179	0.885	0.11689	0.17755	0.88809	0.033
F4	4b	0.221	0.239	0.306	0.22107	0.23350	0.30442	0.047
F5	4b	0.238	0.232	0.631	0.23570	0.23672	0.62591	0.062
F6	4b	0.277	0.331	0.888	0.27962	0.33276	0.88856	0.037
F7	4b	0.295	0.327	0.126	0.29213	0.32708	0.12888	0.035
F8	4b	0.447	0.169	0.645	0.44431	0.17024	0.64859	0.039
F9	4b	0.453	0.165	0.889	0.45332	0.16844	0.88739	0.032
F10	2a	0.000	0	0.000	0.00324	0	0.00503	0.051
F11	2a	0.015	0	0.294	0.01320	0	0.29978	0.058
F12	2a	0.017	0	0.640	0.01116	0	0.63650	0.069
F13	2a	0.225	0	0.763	0.23103	0	0.77255	0.096
F14	2a	0.227	0	0.140	0.22229	0	0.13874	0.060
F15	2a	0.227	0	0.468	0.22432	0	0.47559	0.076
F16	2a	0.514	0	0.323	0.51388	0	0.31332	0.115
F17	2a	0.614	0	0.641	0.61403	0	0.65144	0.125
F18	2a	0.630	0	0.118	0.62210	0	0.12259	0.046
F19	2a	0.728	0	0.472	0.72560	0	0.46301	0.092

Table S6. Experimental (x , y , z)¹¹ and PBE-DFT geometry-optimized (x' , y' , z') fractional atomic coordinates, and corresponding atomic displacements (d , Å) for $\alpha\text{-KY}_3\text{F}_{10}$.

Atom	Site	x	y	z	x'	y'	z'	d
Y1	24e	0.24035	0	0	0.24035	0	0	0.000
K1	8c	1/4	1/4	1/4	1/4	1/4	1/4	0.000
F1	32f	0.11184	0.11184	0.11184	0.11230	0.11230	0.11230	0.009
F2	48i	1/2	0.16574	0.16574	1/2	0.16585	0.16585	0.002

Table S7. Experimental (x , y , z)¹² and PBE-DFT geometry-optimized (x' , y' , z')¹³ fractional atomic coordinates, and corresponding atomic displacements (d , Å) for YF_3 .

Atom	Site	x	y	z	x'	y'	z'	d
Y1	4c	0.3673	1/4	0.0591	0.3687	1/4	0.0604	0.011
F1	4c	0.5227	1/4	0.5910	0.5231	1/4	0.5906	0.003
F2	8d	0.1652	0.06430	0.3755	0.1655	0.0629	0.3775	0.013

Table S8. Compound, Y site and environment, minimum and average Y-F distances (\AA) deduced from ES and APO structures.

Compound	Site	Environment	Y-F		<Y-F>	
			ES	APO	ES	APO
			2.1531	2.1751	2.1610	2.1814
K₂YF₅	Y1	YF ₇	2.2501	2.1905	2.2763	2.2440
KYF₄	Y1	YF ₇	2.1644	2.1612	2.2406	2.2431
	Y2	YF ₇	2.2038	2.2086	2.2469	2.2473
	Y3	YF ₇	2.1532	2.1606	2.2420	2.2441
	Y4	YF ₇	2.2104	2.2160	2.2455	2.2474
	Y5	YF ₇	2.1561	2.1625	2.2403	2.2436
	Y6	YF ₇	2.2076	2.2103	2.2445	2.2487
β-KY₂F₇	Y1	YF ₈	2.1674	2.2034	2.3100	2.3101
	Y2	YF ₈	2.1871	2.1985	2.2501	2.2741
	Y3	YF ₈	2.1617	2.1880	2.2942	2.2716
	Y4	YF ₈	2.1905	2.1999	2.2956	2.2799
	Y5	YF ₈	2.1545	2.1973	2.2748	2.2824
α-KY₃F₁₀	Y1	YF ₈	2.2008	2.2013	2.2776	2.2791
YF₃	Y1	YF ₉	2.2810	2.2751	2.3207	2.3211

Table S9. Compound, K site and environment, minimum and average K-F distances (\AA) deduced from ES and APO structures.

Compound	Site	Environment	F-K		<F-K>	
			ES	APO	ES	APO
			2.6835	/	2.6835	/
γ-K₃YF₆	K1	KF ₆	2.5794	2.5637	2.6188	2.6049
	K2	KF ₈	2.6376	2.6311	2.9062	2.9002
K₂YF₅	K1	KF ₈	2.6125	2.6155	2.7382	2.7472
KYF₄	K1	KF ₈	2.6004	2.6021	2.7719	2.7731
	K2	KF ₈	2.5494	2.5492	2.7870	2.7800
	K3	KF ₈	2.5874	2.5847	2.7942	2.7931
	K4	KF ₈	2.5989	2.5879	2.7804	2.7674
	K5	KF ₈	2.5885	2.6024	2.7524	2.7421
	K6	KF ₈	2.6064	2.6075	2.7898	2.7892
β-KY₂F₇	K1	KF ₁₄	2.5537	2.6438	2.9996	2.9916
	K2	KF ₁₀	2.5717	2.6210	2.7208	2.7436
	K3	KF ₁₀	2.6469	2.6525	2.7397	2.7229
	K4	KF ₁₄	2.5721	2.6547	2.9894	2.9868
α-KY₃F₁₀	K1	KF ₁₆	2.7646	2.7554	3.0909	3.0880

4. ^{19}F MAS NMR of KF-YF₃ binary system

All spectra were reconstructed with the DMFIT¹⁴ software.

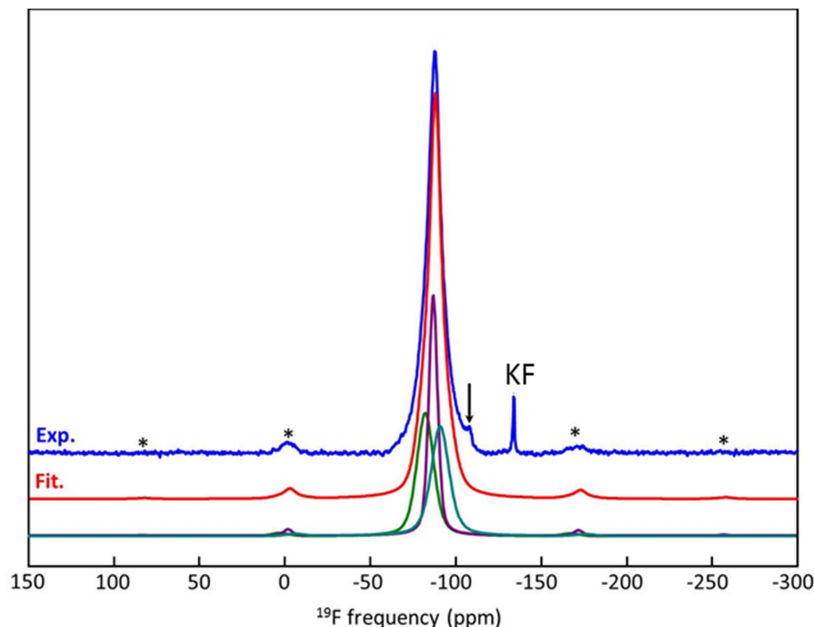


Fig. S4. Experimental (blue) and fitted (red) ^{19}F MAS (60 kHz) NMR (17.6 T) spectra of $\gamma\text{-K}_3\text{YF}_6$. The three individual contributions to the reconstructed spectrum are shown below. The asterisks indicate spinning sidebands. The arrow indicates the presence of an unidentified impurity.

Table S10. ^{19}F isotropic chemical shift (δ_{iso} , ppm), chemical shift anisotropy (δ_{csa} , ppm), asymmetry parameters (η), line width (ppm) and relative intensity (%) determined from reconstruction of the ^{19}F NMR spectrum of $\gamma\text{-K}_3\text{YF}_6$.

Line	δ_{iso} (± 0.1)	δ_{csa} (± 5)	η (± 0.1)	Width (± 0.2)	Intensity (± 1)
1	-82.8	-50	0	11.8	33.4
2	-87.5	-50	0	6.1	33.8
3	-91.5	-45	0	12.6	32.8

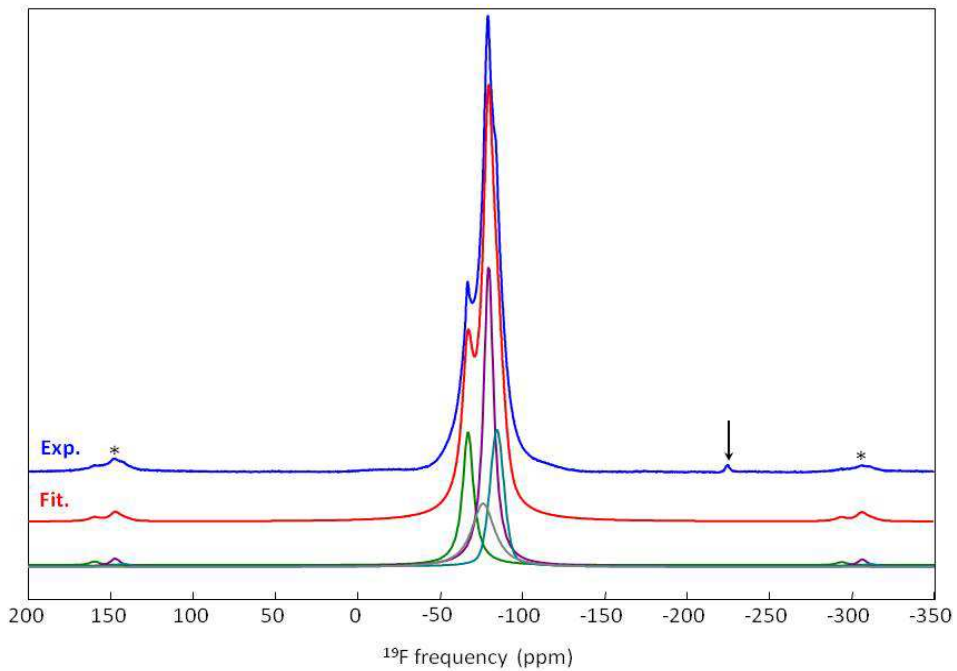


Fig. S5. Experimental (blue) and fitted (red) ^{19}F MAS (64 kHz) NMR (7 T) spectra of K_2YF_5 . The four individual contributions to the reconstructed spectrum are shown below. The asterisks indicate spinning sidebands. The arrow indicates an unidentified impurity.

Table S11. ^{19}F isotropic chemical shift (δ_{iso} , ppm), chemical shift anisotropy (δ_{csa} , ppm), asymmetry parameter (η), line width (ppm) and relative intensity (%) determined from reconstruction of the ^{19}F NMR spectrum of K_2YF_5 .

Line	δ_{iso} (± 0.1)	δ_{csa} (± 10)	η (± 0.1)	Width (± 0.2)	Intensity (± 1)
1	-84.6	-110	0.75	10.0	20.0
2	-79.8	-60	0.65	8.0	40.0
3	-77.0	-100	0.60	16.0	20.0
4	-67.2	-130	0.70	8.1	20.0

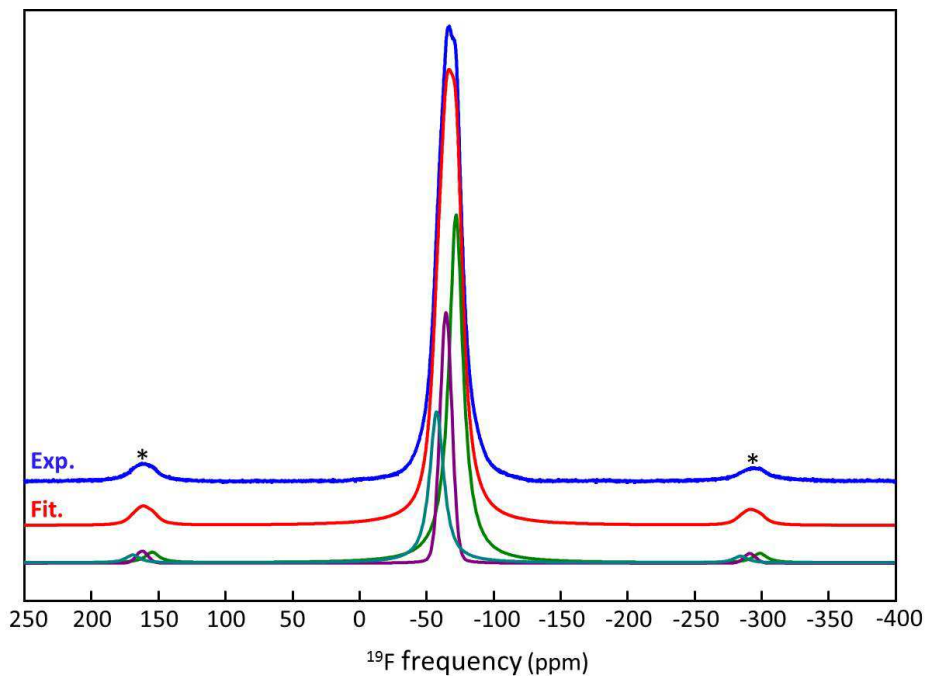


Fig. S6. Experimental (blue) and fitted (red) ^{19}F MAS (64 kHz) NMR (7 T) spectra of KYF_4 . The three individual contributions to the reconstructed spectrum are shown below. The asterisks indicate spinning sidebands.

Table S12. ^{19}F isotropic chemical shift (δ_{iso} , ppm), chemical shift anisotropy (δ_{csa} , ppm), asymmetry parameter (η), line width (ppm) and relative intensity (%) determined from reconstruction of the ^{19}F NMR spectrum of KYF_4 .

Line	δ_{iso} (± 0.1)	δ_{csa} (± 10)	η (± 0.1)	Width (± 0.2)	Intensity (± 1)
1	-72.7	-140	0.5	12.5	50.0
3	-65.4	-170	0.3	10.3	25.0
2	-58.4	-180	0.2	12.5	25.0

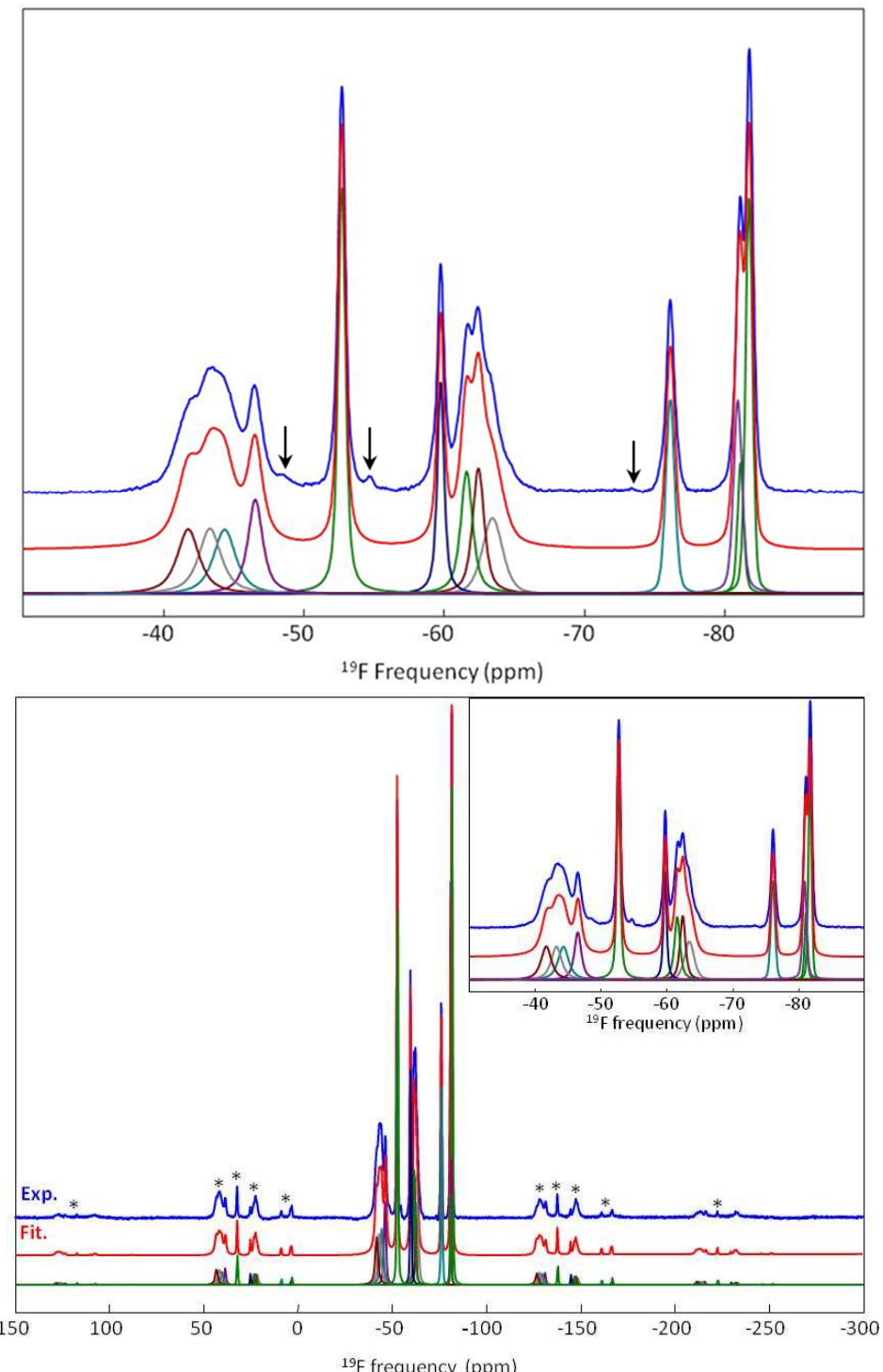


Fig. S7. (Top) ^{19}F “infinite spinning rate” isotropic spectrum issued from the TOP processing of the conventional MAS spectrum and (bottom) experimental (blue) and fitted (red) MAS (60 kHz) NMR (17.6 T) spectra of $\beta\text{-KY}_2\text{F}_7$. The thirteen individual contributions to the reconstructed spectrum are shown below. The asterisks indicate spinning sidebands. The arrows indicate an unidentified impurity.

$\beta\text{-KY}_2\text{F}_7$ structure contains ten F crystallographic sites of multiplicity 2 and nine of multiplicity 4, leading to expected relative intensities of 3.6 and 7.1 % respectively.¹⁰ During spectrum reconstruction, the relative intensities of NMR lines must correspond to ca. 3.6, 7.1 % or any linear combination of these values.

First, the TOP processing was applied to the ^{19}F MAS (60 kHz, 17.6 T) NMR spectrum, to obtain an “infinite spinning frequency” isotropic spectrum.¹⁵ Its careful reconstruction was achieved using thirteen NMR lines and allows us to determine precisely for each the corresponding δ_{iso} , width and relative intensity values.

The reconstruction of the 60 kHz MAS spectrum was then achieved, keeping the δ_{iso} , and width values previously determined, and adjusting the remaining parameters *i.e.* amplitude, chemical shift anisotropy and asymmetry parameters.

Table S13. ^{19}F isotropic chemical shift (δ_{iso} , ppm), chemical shift anisotropy (δ_{csa} , ppm), asymmetry parameter (η), line width (ppm) and relative intensity (%) determined from reconstruction of the ^{19}F NMR spectrum of $\beta\text{-KY}_2\text{F}_7$.

Line	δ_{iso} (± 0.1)	δ_{csa} (± 10)	η (± 0.1)	Width (± 0.2)	Intensity (± 1)
1	-81.8	-45	0	0.6	10.6
2	-81.2	-48	0	0.5	3.3
3	-81.0	-58	0.5	0.7	7.1
4	-76.2	-53	0	0.8	7.2
5	-63.5	-87	0	1.7	7.2
6	-62.5	-112	0.7	1.0	7.1
7	-61.6	-117	0	1.0	7.1
8	-59.8	-78	0	0.6	7.2
9	-52.8	-85	0	0.6	14.3
10	-46.6	-125	0.7	1.3	7.2
11	-44.4	-132	0.75	1.9	7.3
12	-43.4	-136	0.8	1.9	7.2
13	-41.8	-140	0.65	1.9	7.2

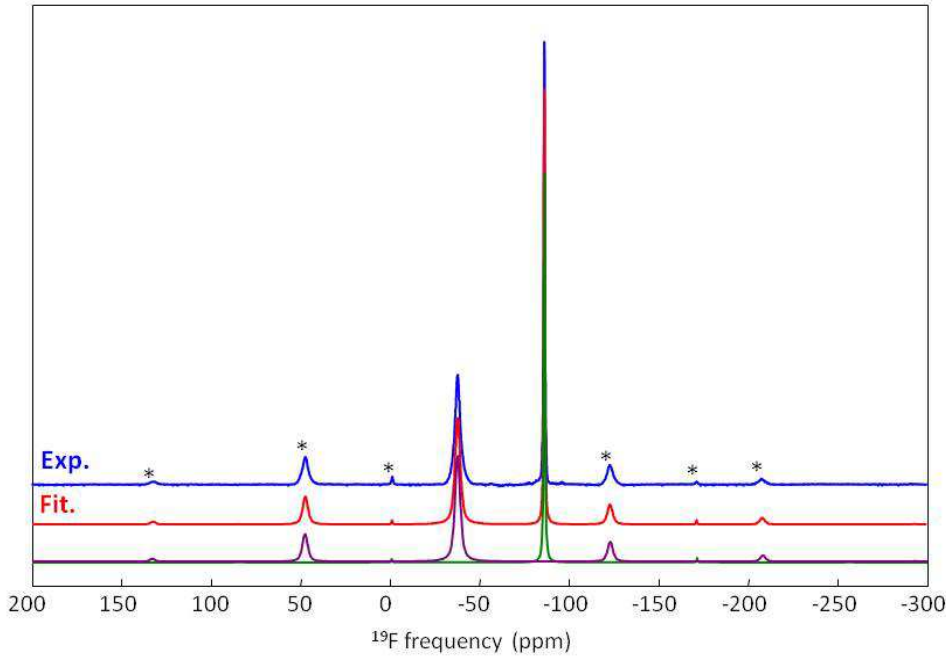


Fig. S8. Experimental (blue) and fitted (red) ^{19}F MAS (60 kHz) NMR (17.6 T) spectra of $\alpha\text{-KY}_3\text{F}_{10}$. The two individual contributions to the reconstructed spectrum are shown below. The asterisks indicate spinning sidebands.

Table S14. ^{19}F isotropic chemical shift (δ_{iso} , ppm), chemical shift anisotropy (δ_{csa} , ppm), asymmetry parameter (η), line width (ppm) and relative intensity (%) determined from reconstruction of the ^{19}F NMR spectrum of $\alpha\text{-KY}_3\text{F}_{10}$.

Line	δ_{iso} (± 0.1)	δ_{csa} (± 10)	η (± 0.1)	Width (± 0.2)	Intensity (± 1)
1	-86.7	28	0.1	0.7	38.9
2	-37.8	-140	0.6	3.7	61.1

Table S15. Phase, F site and multiplicity, ^{19}F σ_{iso} (ppm), σ_{csa} (ppm) and η values issued from DFT-GIPAW calculations for APO structures of KF, $\gamma\text{-K}_3\text{YF}_6$, K_2YF_5 , $\alpha\text{-KY}_3\text{F}_{10}$ and YF_3 and calculated ^{19}F δ_{iso} (ppm) values for $\gamma\text{-K}_3\text{YF}_6$, K_2YF_5 and $\alpha\text{-KY}_3\text{F}_{10}$.

Phase	F site	Mult.	σ_{iso}	δ_{iso}^a	σ_{csa}	η
KF	F1	4b	268.1		0	0
	F2	4e	218.6	-93.9	150.1	0.17
$\gamma\text{-K}_3\text{YF}_6$	F1	4e	210.3	-87.8	151.2	0.20
	F3	4e	207.7	-85.8	134.0	0.25
K_2YF_5	F3	4c	205.8	-84.4	129.1	0.28
	F2	8d	198.3	-78.9	57.1	0.78
	F4	4c	197.1	-77.9	93.1	0.86
	F1	4c	177.0	-63.0	105.3	0.08
$\alpha\text{-KY}_3\text{F}_{10}$	F1	32f	212.2	-89.2	-1.2	0
	F2	48i	143.6	-38.2	174.9	0.61
YF_3	F1	4c	181.3		98.1	0.66
	F2	8d	170.0		-40.8	0.99

^a calculated using the linear correlation: $\delta_{\text{iso},\text{cal}} = -0.743\sigma_{\text{iso}} + 68.5$

Table S16. F site and multiplicity, ^{19}F σ_{iso} (ppm), σ_{csa} (ppm) and η values issued from DFT-GIPAW calculations for APO structures of $\beta\text{-KY}_2\text{F}_7$.

F site	Mult	σ_{iso}	σ_{csa}	η
F13	2a	207.1	19.3	0.42
F10	2a	205.1	21.7	0.53
F1	4b	204.7	14.0	0.78
F5	4b	203.0	17.3	0.77
F11	2a	195.4	24.8	0.91
F15	2a	195.1	-27.2	0.68
F12	2a	175.7	66.4	0.63
F7	4b	174.9	141.3	0.56
F14	2a	174.7	59.5	0.64
F8	4b	170.1	151.5	0.57
F19	2a	167.5	57.5	0.42
F2	4b	166.4	88.5	0.42
F16	2a	166.4	52.2	0.34
F4	4b	164.9	91.7	0.26
F17	2a	156.5	164.0	0.52
F18	2a	153.3	169.2	0.50
F3	4b	150.9	171.7	0.52
F9	4b	149.6	172.7	0.61
F6	4b	148.4	174.5	0.60

Table S17. F site, cationic environment, ^{19}F σ_{iso} (ppm) and calculated δ_{iso} (ppm), σ_{csa} (ppm) and η values issued from DFT-GIPAW calculations for APO structures of KYF_4 .

F site	Env.	σ_{iso}	δ_{iso}^a	σ_{csa}	η
F19	2Y-2K	195.2	-76.5	44.0	0.87
F10	2Y-2K	194.6	-76.1	146.0	0.33
F1	2Y-2K	193.8	-75.5	145.5	0.34
F9	2Y-2K	193.1	-75.0	159.8	0.09
F16	2Y-2K	193.0	-74.9	44.5	0.73
F2	2Y-2K	192.6	-74.6	157.6	0.12
F5	2Y-2K	192.3	-74.4	145.5	0.37
F6	2Y-2K	191.0	-73.3	162.8	0.06
F23	2Y-2K	191.1	-73.5	48.8	0.69
F20	1Y-3K	189.2	-72.1	154.9	0.23
F24	1Y-3K	186.9	-70.4	153.9	0.22
F22	2Y-2K	186.7	-70.2	45.1	0.59
F15	1Y-3K	186.3	-69.9	152.5	0.18
F14	2Y-2K	184.1	-68.2	48.5	0.63
F17	2Y-2K	181.9	-66.7	46.2	0.51
F13	1Y-3K	180.1	-65.2	141.8	0.33
F21	1Y-3K	179.6	-64.9	141.0	0.28
F18	1Y-3K	178.9	-64.5	138.7	0.29
F12	2Y-1K	174.7	-61.3	169.2	0.25
F8	2Y-1K	173.1	-60.1	144.5	0.20
F7	2Y-1K	173.0	-60.0	177.3	0.23
F3	2Y-1K	172.5	-59.7	142.8	0.22
F11	2Y-1K	171.1	-58.6	144.9	0.21
F4	2Y-1K	171.1	-58.6	184.1	0.23

^a calculated using the linear correlation: $^{19}\text{F} \delta_{\text{iso},\text{calc}} = -0.743\sigma_{\text{iso}} + 68.5$

5. ^{89}Y MAS NMR of KF-YF₃ binary system

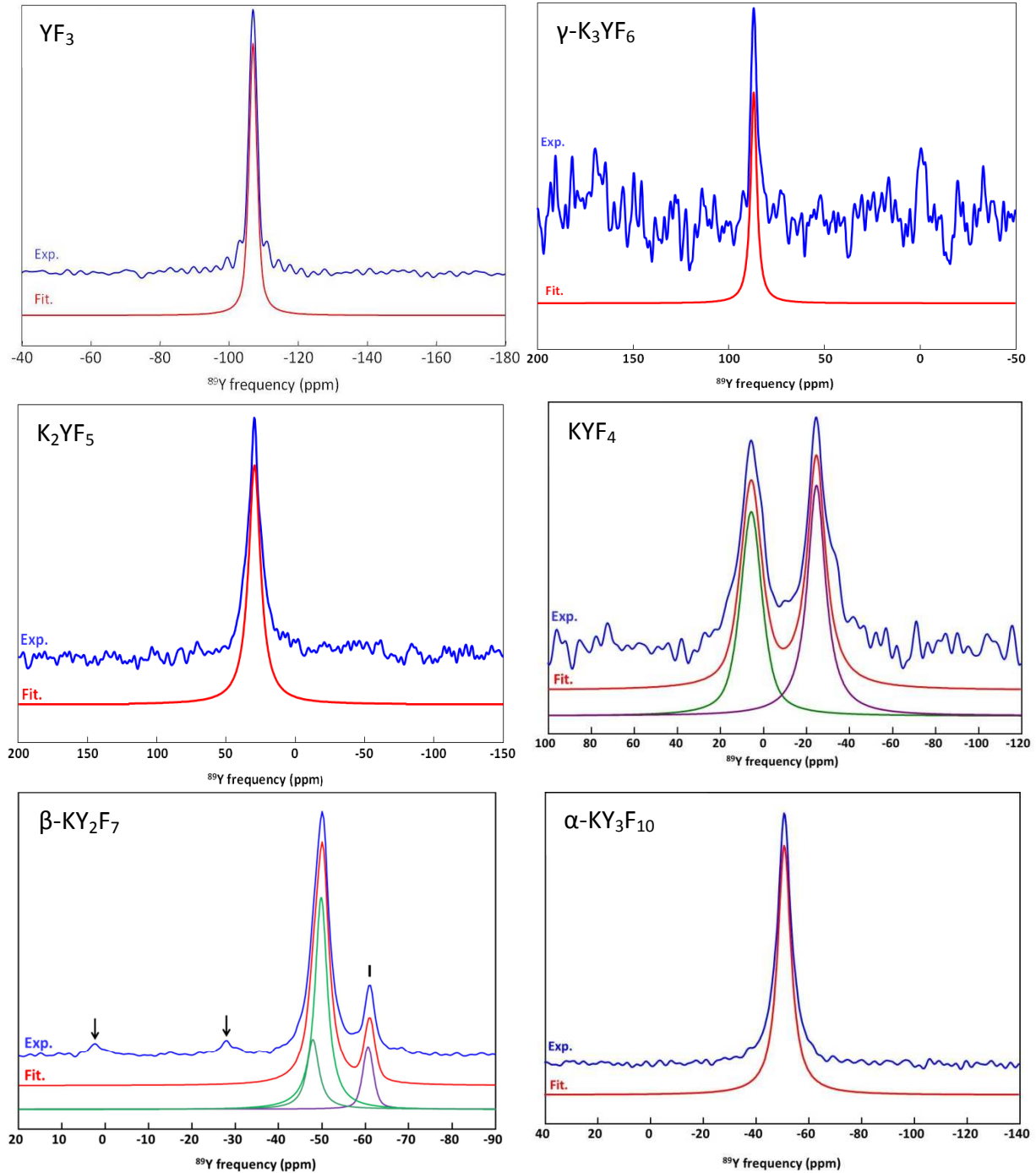


Fig. S9. Experimental (blue) and fitted (red) ^{89}Y MAS (3 kHz) NMR (7 T) spectrum of YF₃, $\gamma\text{-K}_3\text{YF}_6$, K₂YF₅, KYF₄, $\beta\text{-KY}_2\text{F}_7$, and $\alpha\text{-KY}_3\text{F}_{10}$. The individual contributions to the reconstructed spectrum are shown below. The arrows indicate the presence of KYF₄ as impurity.

Table S18. Phase, NMR line, ^{89}Y δ_{iso} (ppm), line width (ppm) and relative intensity (%) determined from reconstruction of the ^{89}Y NMR spectra of KF-YF₃ binary system.

Phase	Line	δ_{iso} (± 0.5)	Width (± 0.2)	Intensity (± 1)
$\gamma\text{-K}_3\text{YF}_6$	1	86.9	3.9	100
K ₂ YF ₅	1	29.7	10.5	100
KYF ₄	1	-28.5	10.3	50.4
	2	2.1	11.0	49.6
$\beta\text{-KY}_2\text{F}_7$	1	-60.6	2.9	13.7
	2	-49.8	3.4	65.8
	3	-47.9	3.3	20.5
$\alpha\text{-KY}_3\text{F}_{10}$	1	-50.8	6.1	100
YF ₃	1	-107.0	2.7	100

6. ^{39}K NMR

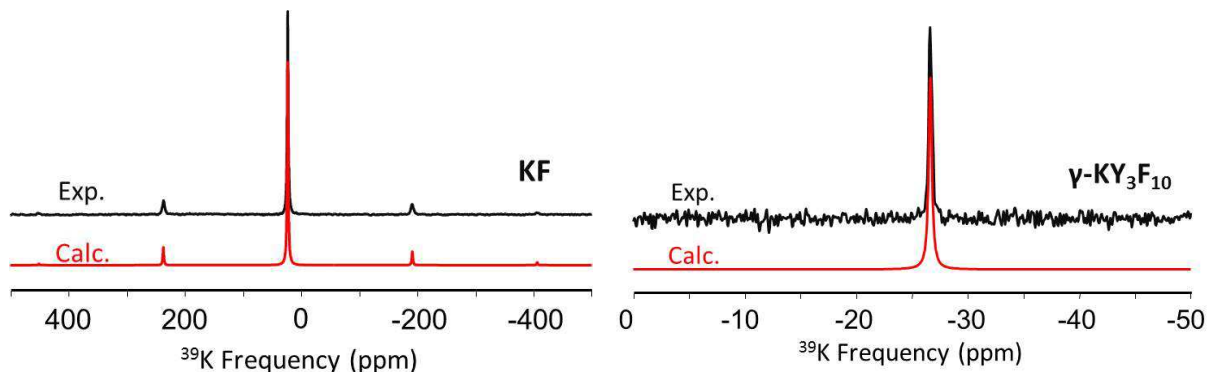


Fig. S10. Experimental (black) and fitted (red) ^{39}K MAS (3 kHz) NMR of KF and $\alpha\text{-KY}_3\text{F}_{10}$.

Table S19. Phase, K site, ^{39}K EFG tensor components ($V_{ij}, 10^{21} \text{ V/m}^2$) and Euler angle values ($^\circ$) issued from DFT-GIPAW calculations for APO structures.

Phase	K site	V_{xx}	V_{yy}	V_{zz}	α	β	γ
$\gamma\text{-K}_3\text{YF}_6$	K1	0.267	0.743	-1.010	-94	15	88
	K2	0.408	0.916	-1.324	-84	8	-132
K_2YF_5	K1	-0.207	-1.149	1.356	20	82	-155
KYF_4	K1	-0.512	-1.511	2.023	137	1	37
	K2	-0.798	-1.914	2.712	81	172	97
	K3	-0.607	-1.813	2.421	96	174	-83
	K4	-0.557	-1.583	2.140	124	6	-97
	K5	-0.577	-1.593	2.170	-81	3	-109
	K6	-0.848	-1.559	2.407	111	9	101
$\beta\text{-KY}_2\text{F}_7$	K1	0.238	0.522	-0.760	-90	180	90
	K2	0.310	0.800	-1.111	0	8	180
	K3	0.187	0.567	-0.754	180	170	180
	K4	0.366	0.485	-0.851	90	5	-90

Table S20. Eigenvectors of the calculated ^{39}K EFG tensor, expressed in the crystallographic axis, for K1 in K_2YF_5 (APO), K1 and K2 in $\gamma\text{-K}_3\text{YF}_6$ (APO), and K2 in KYF_4 (APO).

Compound	Site	Axis	V_{xx}	V_{yy}	V_{zz}
K_2YF_5	K1	a	0.0875	0.0280	-0.0116
		b	-0.0447	0.113	-0.0643
		c	$-5.85 \cdot 10^{-3}$	0.0731	0.133
$\gamma\text{-K}_3\text{YF}_6$	K1	a	0.0996	-0.0855	0.0876
		b	-0.0305	0.0884	0.121
		c	0.0837	0.0668	-0.0278
	K2	a	-0.114	0.0496	-0.0967
		b	0.0855	-0.0382	-0.121
		c	0.0435	0.102	$-1.37 \cdot 10^{-3}$
KYF_4	K2	a	-0.0591	0.0521	-0.0209
		b	-0.0158	0.0143	-0.0787
		c	0.0648	0.0737	$4.22 \cdot 10^{-4}$

Table S21. F-K1-F angles ($^{\circ}$) between two adjacent K-F bonds for $K1F_6$ octahedron in APO structure of γ - K_3YF_6 .

Atom	Atom	Angle
F1	F3	83.6
F1	F3	96.4
F1	F2	90.2
F1	F2	89.8
F1	F3	96.4
F1	F3	83.6
F1	F2	89.8
F1	F2	90.2
F3	F2	85.2
F3	F2	94.8
F3	F2	94.8
F3	F2	85.2

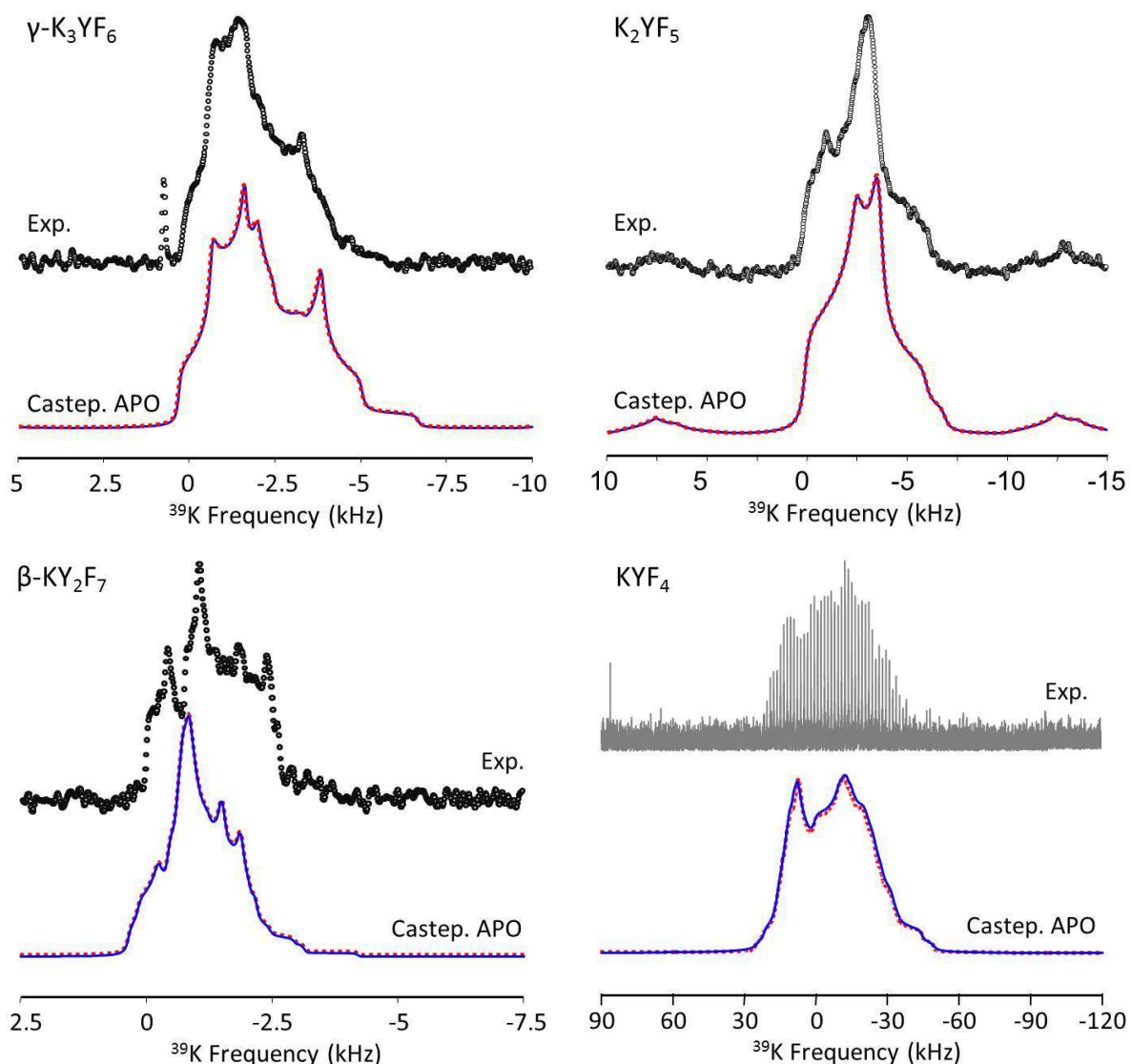


Fig. S11. Experimental (black) and theoretical ^{39}K MAS NMR (17.6 T) spectra of γ - K_3YF_6 , K_2YF_5 , β - KY_2F_7 and KYF_4 . Theoretical spectra are obtained using CASTEP quadrupolar parameter values with (blue) or without (dashed red) δ_{csa} and Euler angles.

References

- [1] Y. A. Kharitonov, Y. A. Gorbunov and B. A. Maksimov, *Kristallogr.*, 1983, **28**, 1031–1032.
- [2] N. M. Khaidukov, P. P. Fedorov, L. N. Demyanets, I. P. Zibrov and V. A. Malyusov, *Russ. J. Inorg. Chem.*, 1990, **35**, 383–384.
- [3] F. Loncke, D. Zverev, H. Vrielinck, N. M. Khaidukov, P. Matthys and F. Callens, *Phys. Rev. B.*, 2007, **75**, 144427.
- [4] K. Güde and C. Hebecker, *Z. Naturforsch.*, 1985, **40B**, 864–867.
- [5] I. D. Brown and D. Altermatt, *Acta Crystallogr., Sect. B: Struct. Sci.*, 1985, **41**, 244–247.
- [6] N. E. Brese and M. O’Keeffe, *Acta Crystallogr., Sect. B: Struct. Sci.*, 1991, **47**, 192–197.
- [7] G. Finch and S. Fordham, *Proc. Phys. Soc.*, 1936, **48**, 85–94.
- [8] M. A. Gusowski, A. Gągor, M. Trzebiatowska-Gusowska, W. Ryba-Romanowski, *J. Solid State Chem.*, 2006, **179**, 3145–3150.
- [9] A. Grzechnik, N. Khaidukovb, K. Friesec, *Dalton Trans.*, 2013, **42**, 441–447.
- [10] E. I. Ardashnikova, M. P. Borzenkova and A. V. Novoselova, *Russ. J. Inorg. Chem.*, 1980, **25**, 833–836.
- [11] A. Grzechnik, J. Nuss, K. Friese, J.-Y. Gesland, M. Jansen, *Z. Kristallogr. New Cryst. Struct.*, 2002, **217**, 460–460.
- [12] A. K. Cheetham, N. Norman, *Acta Chem. Scand., Ser. A.*, 1974, **28**, 55–60.
- [13] A. Sadoc, M. Body, C. Legein, M. Biswal, F. Fayon, X. Rocquefelte and F. Boucher, *Phys. Chem. Chem. Phys.*, 2011, **13**, 18539–18550.
- [14] D. Massiot, F. Fayon, M. Capron, I. King, S. Le Calvé, B. Alonso, J.-O. Durand, B. Bujoli, Z. Gan and G. Hoatson, *Magn. Reson. Chem.*, 2002, **40**, 70–76.
- [15] D. Massiot, J. Hiet, N. Pellerin, F. Fayon, M. Deschamp, S. Steuernagel, P. J. Grandinetti, *J. Magn. Reson.*, 2006, **181**, 310–315.